Supporting Information

Wang et al. 10.1073/pnas.1219683110

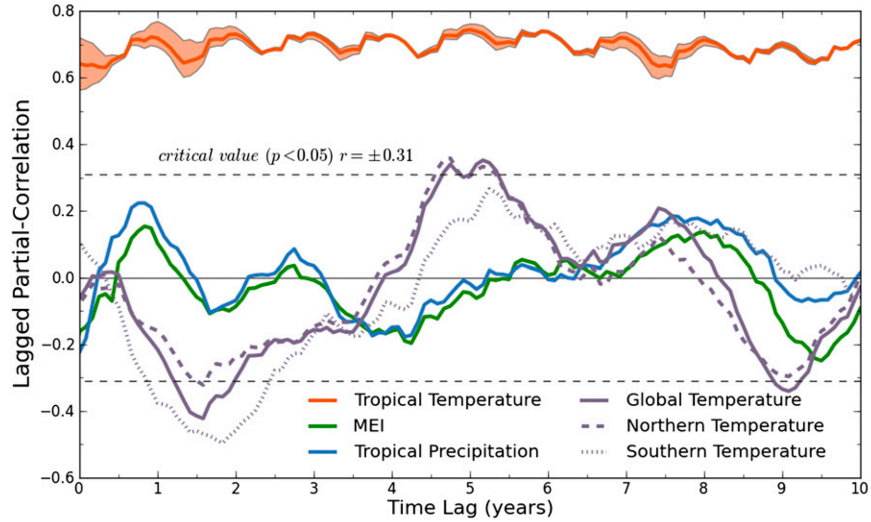

Fig. S1. Partial correlations between the atmospheric CO_2 growth rate, the concurrent tropical land-surface temperature, and other climate variables at various time lags. A partial correlation represents the correlation between two variables with the possible effects of a third (control) variable on them being excluded (1). Specifically, the partial correlations between the CO_2 growth rate and the concurrent tropical land temperature are calculated with one of the five other lagged climate variables alternately used as the control variable, resulting in a set of five partial-correlation values at every time lag (of the control variables). The mean and the range of the partial correlations between the CO_2 growth rate and the concurrent tropical temperature are indicated by the orange line and the orange shading, respectively. In comparison, the partial correlations between CO_2 growth rate and each of the five other lagged climate variables are calculated with the concurrent tropical land temperature as the control variable. Note that the tropical temperature is fixed at a time lag of 0 y (i.e., concurrent with the CO_2 growth rate), so that the horizontal axis (i.e., "abscissa") indicates only the time lags in the other five climate variables. The definitions of the spatial extents (e.g., "tropical," "northern," "southern," and "global") are the same as in Fig. 2. Also, the critical values for the correlations at 95% significance levels ($P < 0.05$) are estimated by the same methods as described in Fig. 2.

1. Kendall MG, Stuart A (1979) *The Advanced Theory of Statistics: Inference and Relationship* (Charles Griffin, London), 4th Ed, Vol 2.

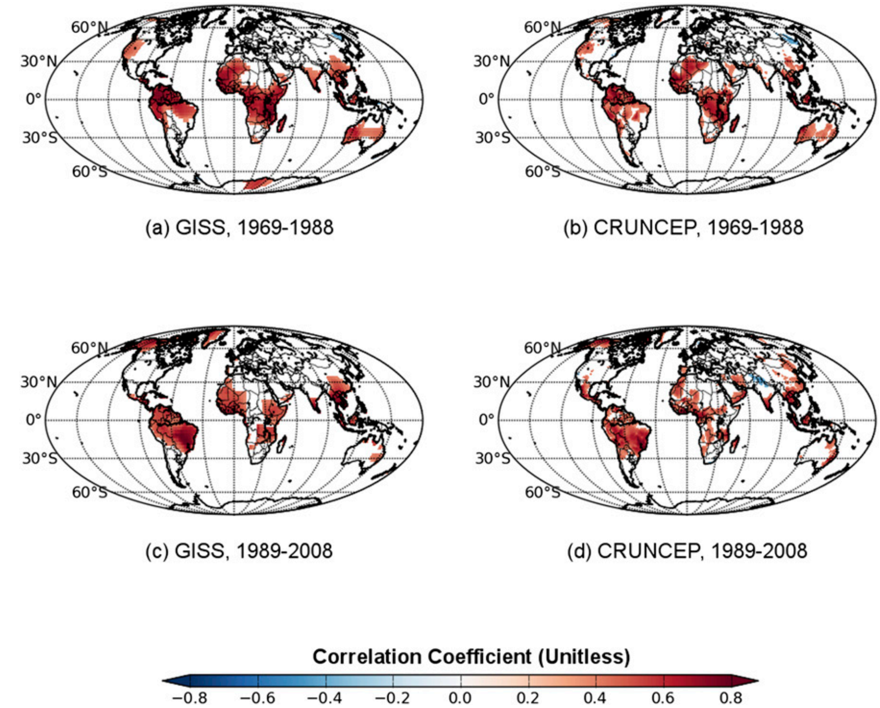

Fig. S2. Correlations between detrended anomalies of the atmospheric CO_2 growth rate and Goddard Institute for Space Studies (GISS) (1) surface temperatures (*A* and *C*) and Climatic Research Unit–National Centers for Environmental Prediction (CRUNCEP) (2, 3) surface temperatures (*B* and *D*) for 1969 to 1988 (*A* and *B*) and for 1989 to 2008 (*C* and *D*). Only correlation coefficients significant at 90% level ($P < 0.1$) are shown. Note that, for 1989 to 2008, there are missing data in Goddard Institute for Space Studies temperatures over some regions of Africa (*C*).

1. Hansen J, Ruedy R, Glascoe J, Sato M (1999) GISS analysis of surface temperature change. *J Geophys Res* 104:30997–31022.
2. Sitch S, et al. (2008) Evaluation of the terrestrial carbon cycle, future plant geography and climate-carbon cycle feedbacks using five Dynamic Global Vegetation Models (DGVMs). *Glob Change Biol* 14:2015–2039.
3. Le Quéré C, et al. (2009) Trends in the sources and sinks of carbon dioxide. *Nat Geosci* 2:831–836.

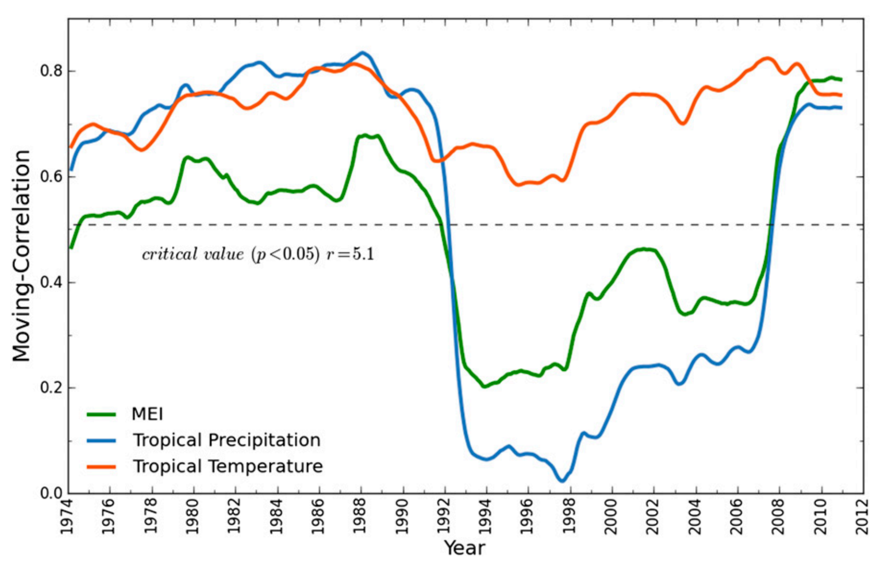

Fig. S3. Moving correlations of atmospheric CO_2 growth rate with tropical land-surface air temperature, tropical land precipitation, and the Multivariate El Niño–Southern Oscillation Index (MEI) with a 15-y time window. The time label of the correlation coefficients indicates the last year of the time window (i.e., *r* value for 2010 represents the correlation coefficient of the two variables between 1996 and 2010). The time series of MEI and tropical precipitation are shifted by 6 mo to account for the time lags of their correlations with the CO_2 growth rate (Fig. 2). The significant changes of the correlations between the CO_2 growth rate and the tropical precipitation or MEI during 1992 to 2008 mainly reflect the decoupling of the variables in 1991 to 1994 (Fig. 1) and are explained in the main text.

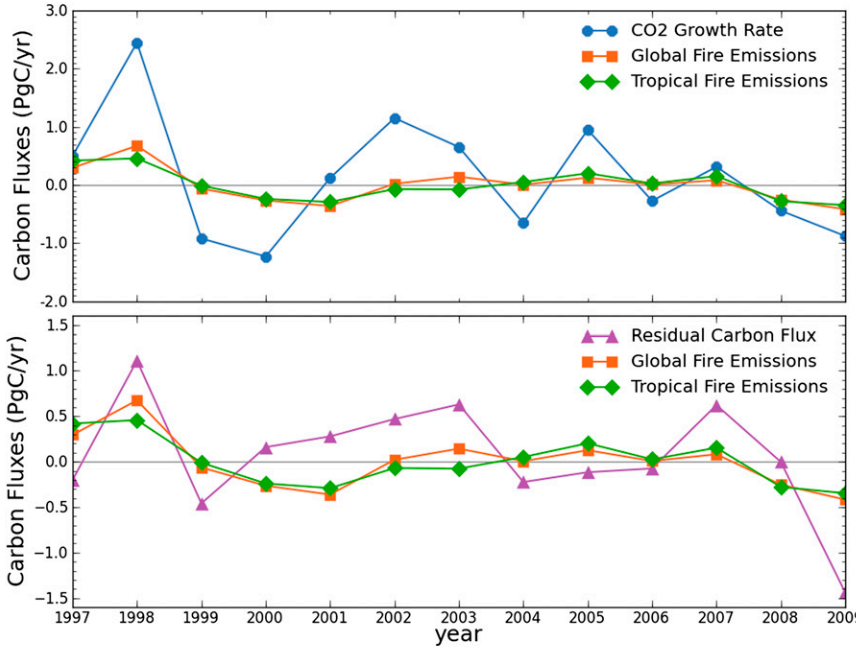

Fig. S4. Anomalies of annual fire CO_2 emissions (Global Fire Emissions Database Version 3) (1) compared with the detrended anomalies of the atmospheric CO_2 growth rate (*Upper*) and the residual carbon flux (*Lower*). The annual anomalies of the CO_2 growth rate and the residual carbon fluxes are subsampled from the corresponding time series shown in Figs. 1 and 4. As shown, the overall SD (σ) of global or tropical fire emission anomalies (~0.26 PgC/y) is small compared with those of the CO_2 growth rate and the residual carbon anomalies (1.0 PgC/y and 0.7 PgC/y, respectively). Also, the variability of fire emissions has its own characteristics, which occasionally show large anomalies in extreme years (e.g., 1997–1998) but remain rather constant during other periods (e.g., 2002–2007). Not all such variability can be explained by tropical temperature anomalies. As a result, the fire emission anomalies are significantly correlated ($r \sim 0.6$) with the residual carbon fluxes.

1. van der Werf GR (2010) Global fire emissions and the contribution of deforestation, savanna, forest, agricultural, and peat fires (1997-2009). *Atmos Chem Phys* 10:11707–11735.

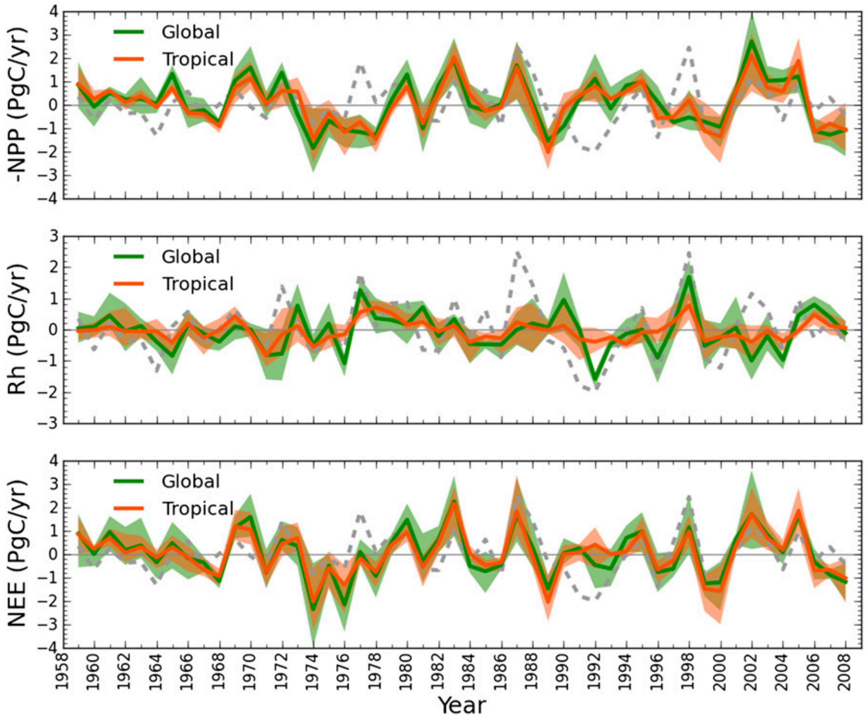

Fig. S5. Detrended net primary production (NPP; i.e., with its sign of values reversed), heterotrophic respiration (Rh), and net ecosystem exchange (NEE) originally simulated by the Dynamic Global Vegetation Model experiment previously described (1, 2). The color shades represent the spread among the models, and the solid lines represent the ensemble mean. The gray dashed line represents the time series of observed atmospheric CO_2 growth rate, subsampled from the corresponding time series shown in Fig. 1. The results show the tropical dominance in regulating the variability of global carbon fluxes. The SDs of the simulated carbon fluxes and their correlations with the CO_2 growth rate or tropical climate variables are summarized in Tables S1 and S2 (by the "non-optimized" values).

1. Sitch S, et al. (2008) Evaluation of the terrestrial carbon cycle, future plant geography and climate-carbon cycle feedbacks using five Dynamic Global Vegetation Models (DGVMs). *Glob Change Biol* 14:2015–2039.
2. Le Quéré C, et al. (2009) Trends in the sources and sinks of carbon dioxide. *Nat Geosci* 2:831–836.

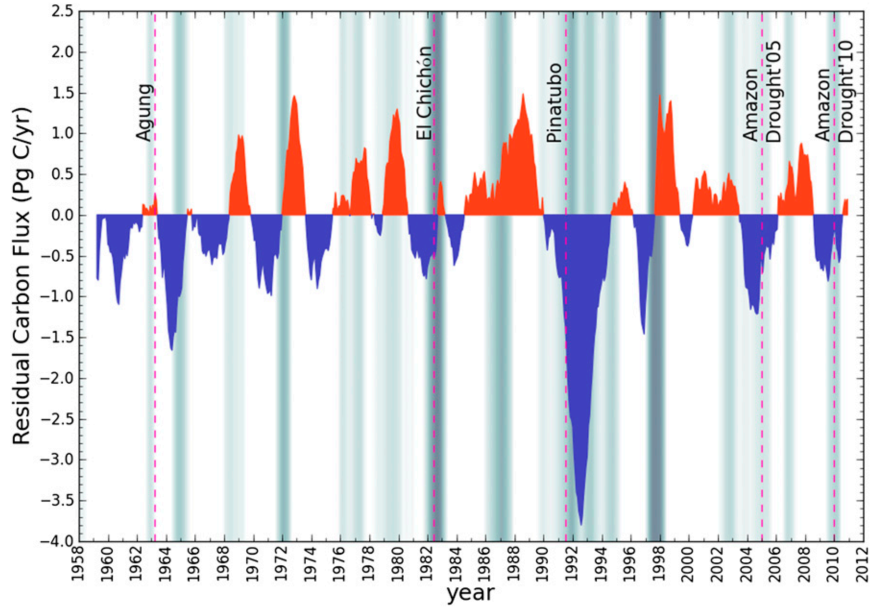

Fig. S6. Same as Fig. 4 but with the residual carbon flux anomalies estimated by the differences between the observed atmospheric CO_2 growth rates and those estimated from tropical land precipitation anomalies with a linear regression model that emphasizes the "normal" relationship between the two fields. That is, we first estimated the linear regression relationship between the CO_2 growth rate and tropical precipitation by masking out their anomalies during 1991 to 1994, which significantly deviated from their coupling during other periods (Fig. 1 and Fig. S2). We then applied the obtained linear relationship to the whole precipitation records (including 1991–1994) to estimate the expected CO_2 growth rates and compared the estimates with the observations. The residual carbon fluxes calculated in this fashion minimize the differences between the observed and the estimated CO_2 growth rate under normal conditions but highlight their inconsistency during 1991 to 1994. As shown, the negative residual anomalies (i.e., extra carbon sink) estimated for this period have a magnitude (absolute value, hereafter the same) over 3.5 PgC/y, more than two times as large as any other residual anomalies in the 50-y data records. They are also significantly larger than the corresponding residual anomalies estimated from the coupling between atmospheric CO_2 growth rate and tropical land-surface temperatures (~1.7 PgC/y; Fig. 4, which does not significantly change with or without the 1991–1994 anomalies masked out in the regression analysis). Such an intense extra carbon sink is very difficult to explain by previously proposed biogeophysical factors that occurred around 1991 to 1994 (as discussed in the text) and raises questions regarding whether the normal coupling between tropical precipitation and the CO_2 growth rate truly reflects the sensitivity of tropical NEE to interannual precipitation variations.

Table S1. SDs of interannual variations of tropical carbon fluxes

	SD, PgC/y		
Simulation	NPP	Rh	NEE
LPJ	0.97 (0.44)	0.54 (0.43)	1.03 (0.56)
HyLand	0.52 (0.41)	0.49 (0.61)	0.44 (0.48)
SHE	1.00 (0.37)	0.30 (0.15*)	0.96 (0.36)
TRIFFID	1.42 (0.33)	0.42 (0.55)	1.54 (0.68)
Mean	0.92 (0.42)	0.32 (0.55)	0.93 (0.65)

Sources of simulations are as follows: HyLand (1), LPJ (2), SHE (3), and TRIFFID (4) from the model experiments described previously (5, 6). Mean indicates the ensemble mean of the models. The simulated tropical carbon fluxes include NPP, Rh, and NEE. Values in parentheses represent "optimal" variability of the corresponding variables estimated through regression analysis to minimize the deviations of the resulting NEE from the observed atmospheric CO_2 growth rate. Note that, in the regression analysis, we treat the ensemble mean as an individual model. LPJ, Lund–Potsdam–Jena Dynamic Global Vegetation Model; NEE, net ecosystem exchange; NPP, net primary production; Rh, heterotrophic respiration; SHE, Sheffield–Dynamic Global Vegetation Model; TRIFFID, Top-down Representation of Interactive Foliage and Flora Including Dynamics Dynamic Global Vegetation Model.

*The scaling coefficient for this variable is statistically nonsignificant.

1. Friend AD, White A (2000) Evaluation and analysis of a dynamic terrestrial ecosystem model under preindustrial conditions at the global scale. *Global Biogeochem Cycles* 14:1173–1190.
2. Sitch S, et al. (2003) Evaluation of ecosystem dynamics, plant geography and terrestrial carbon cycling in the LPJ dynamic vegetation model. *Glob Change Biol* 9:161–185.
3. Woodward FI, Lomas MR (2004) Vegetation dynamics—simulating responses to climatic change. *Biol Rev Camb Philos Soc* 79(3):643–670.
4. Cox PM (2001) *Description of the "TRIFFID" Dynamic Global Vegetation Model*. Hadley Centre Technical Note 24 (United Kingdom Meteorological Office, Bracknell, UK).
5. Sitch S, et al. (2008) Evaluation of the terrestrial carbon cycle, future plant geography and climate-carbon cycle feedbacks using five Dynamic Global Vegetation Models (DGVMs). *Glob Change Biol* 14:2015–2039.
6. Le Quéré C, et al. (2009) Trends in the sources and sinks of carbon dioxide. *Nat Geosci* 2:831–836.

Table S2. Correlations of simulated tropical NEE with tropical land-surface air temperature, land precipitation, and atmospheric CO_2 growth rate

	r of NEE		
Simulation	Temperature	Precipitation	CO_2
LPJ	0.80 (0.81)	−0.55 (−0.31)	0.55 (0.58)
HyLand	0.75 (0.69)	−0.76 (−0.63)	0.45 (0.50)
SHE	0.67 (0.68)	−0.78 (−0.74)	0.38 (0.38)
TRIFFID	0.83 (0.90)	−0.77 (−0.46)	0.56 (0.71)
Mean	0.82 (0.90)	−0.76 (−0.39)	0.53 (0.67)

Sources of simulations are as follows: HyLand (1), LPJ (2), SHE (3), and TRIFFID (4) from the model experiments described previously (5, 6). As in Table S1, values in parentheses represent "optimal" correlations estimated through regression analysis. LPJ, Lund–Potsdam–Jena Dynamic Global Vegetation Model; NEE, net ecosystem exchange; SHE, Sheffield–Dynamic Global Vegetation Model; TRIFFID, Top-down Representation of Interactive Foliage and Flora Including Dynamics Dynamic Global Vegetation Model.

1. Friend AD, White A (2000) Evaluation and analysis of a dynamic terrestrial ecosystem model under preindustrial conditions at the global scale. *Global Biogeochem Cycles* 14:1173–1190.
2. Sitch S, et al. (2003) Evaluation of ecosystem dynamics, plant geography and terrestrial carbon cycling in the LPJ dynamic vegetation model. *Glob Change Biol* 9:161–185.
3. Woodward FI, Lomas MR (2004) Vegetation dynamics—simulating responses to climatic change. *Biol Rev Camb Philos Soc* 79(3):643–670.
4. Cox PM (2001) *Description of the "TRIFFID" Dynamic Global Vegetation Model*. Hadley Centre Technical Note 24 (UK Meteorological Office, Bracknell, UK).
5. Sitch S, et al. (2008) Evaluation of the terrestrial carbon cycle, future plant geography and climate-carbon cycle feedbacks using five Dynamic Global Vegetation Models (DGVMs). *Glob Change Biol* 14:2015–2039.
6. Le Quéré C, et al. (2009) Trends in the sources and sinks of carbon dioxide. *Nat Geosci* 2:831–836.